BIOCHEMISTRY
including biophysical chemistry & molecular biology

Article

pubs.acs.org/biochemistry

Electron Transfer Mechanism of the Rieske Protein from *Thermus thermophilus* from Solution Nuclear Magnetic Resonance Investigations

Kuang-Lung Hsueh,[†] Marco Tonelli,[‡] Kai Cai,[§] William M. Westler,[‡] and John L. Markley*[,‡,§]

[†]Graduate Program in Biophysics, [‡]National Magnetic Resonance Facility at Madison, and [§]Department of Biochemistry, 433 Babcock Drive, University of Wisconsin, Madison, Wisconsin 53706, United States

Supporting Information

ABSTRACT: We report nuclear magnetic resonance (NMR) data indicating that the Rieske protein from the cytochrome *bc* complex of *Thermus thermophilus* (*Tt*Rp) undergoes modest redox-state-dependent and ligand-dependent conformational changes. To test models concerning the mechanism by which *Tt*Rp transfers between different sites on the complex, we monitored ^{1}H, ^{15}N, and ^{13}C NMR signals as a function of the redox state and molar ratio of added ligand. Our studies of full-length *Tt*Rp were conducted in the presence of dodecyl phosphocholine micelles to solvate the membrane anchor of the protein and the hydrophobic tail of the ligand (hydroubiquinone). NMR data indicated that hydroubiquinone binds to *Tt*Rp and stabilizes an altered protein conformation. We utilized a truncated form of the Rieske protein lacking the membrane anchor (trunc-*Tt*Rp) to investigate redox-state-dependent conformational changes. Local chemical shift perturbations suggested possible conformational changes at prolyl residues. Detailed investigations showed that all observable prolyl residues of oxidized trunc-*Tt*Rp have *trans* peptide bond configurations but that two of these peptide bonds (Cys151−Pro152 and Gly169−Pro170 located near the iron−sulfur cluster) become *cis* in the reduced protein. Changes in the chemical shifts of backbone signals provided evidence of redox-state- and ligand-dependent conformational changes localized near the iron−sulfur cluster. These structural changes may alter interactions between the Rieske protein and the cytochrome *b* and *c* sites and provide part of the driving force for movement of the Rieske protein between these two sites.

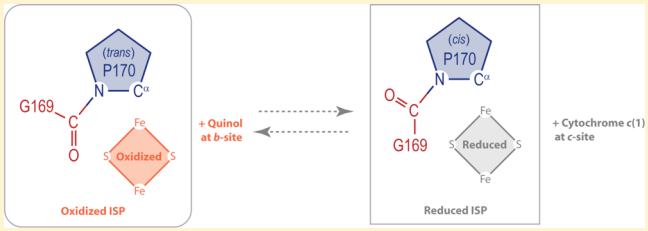

Thermus thermophilus Rieske protein (*Tt*Rp) is a catalytic subunit of the bacterial cytochrome *bc* complex. The biological function of the cytochrome $bc_{(1)}$ complex (EC 1.10.2.2) is to transfer electrons from hydroquinone to cytochrome $c_{(1)}$, to pump protons across the membrane, and to store the energy as a chemiosmotic potential.[1−5] The electron transfer mechanism is known as the bifurcated Q-cycle.[6−10] The Rieske protein serves as a carrier of electrons and protons between hydroquinone and cytochrome $c_{(1)}$. A homologous Rieske protein has similar functions in the cytochrome b_6f complex. The cytochrome $bc_{(1)}$ complex consists of three key subunits with cofactors: cytochrome *b* with diheme, cytochrome $c_{(1)}$ with a heme, and the Rieske iron−sulfur protein with a [2Fe-2S] cluster. In *T. thermophilus*, all subunits contain at least one membrane domain anchored on the inner membrane. On the basis of X-ray crystal structures of related proteins,[1,2] the $bc_{(1)}$ complex contains two primary binding sites for the Rieske protein: one, called the *b*-site, is close to cytochrome *b*, and the other, called the *c*-site, is close to cytochrome $c_{(1)}$. Hydroquinones are oxidized in the *b*-site. After proton and electron transfer at the *b*-site, the Rieske protein moves to the *c*-site, where it donates an electron to cytochrome $c_{(1)}$.[1,2] Increased viscosity, which presumably slows movement of the Rieske protein between the two sites, was found to impede the rate of electron transfer and to be part of the rate-limiting process because of the large distance between the cytochrome *b* and $c_{(1)}$ sites.[11]

Several models have been advanced to explain the mechanism by which the Rieske protein (ISP) moves. Their features are summarized in Table S1 (Supporting Information). These models can be classified as being driven by a conformational change (model 1) or being driven by diffusion (model 2) as discussed below.

In model 1, the multiple conformations of the Rieske protein observed in different X-ray crystal structures suggested that large redox-state-coupled and/or ligand-coupled conformational changes promote transfer between the two sites.[1,12−14] The two putative regions undergoing conformational changes are the iron−sulfur cluster binding domain[15,16] and the neck domain (also called the linker or tether domain).[17] Figure 1 illustrates the proposed movements and/or conformational changes. When the ISP is located at the hydroquinone binding site (*b*-site), its neck domain does not form a helix (Figure 1A). When the head domain (soluble domain) of the Rieske protein moves to the intermediate site (*int*-site), the neck domain

Received: March 7, 2013
Published: March 12, 2013

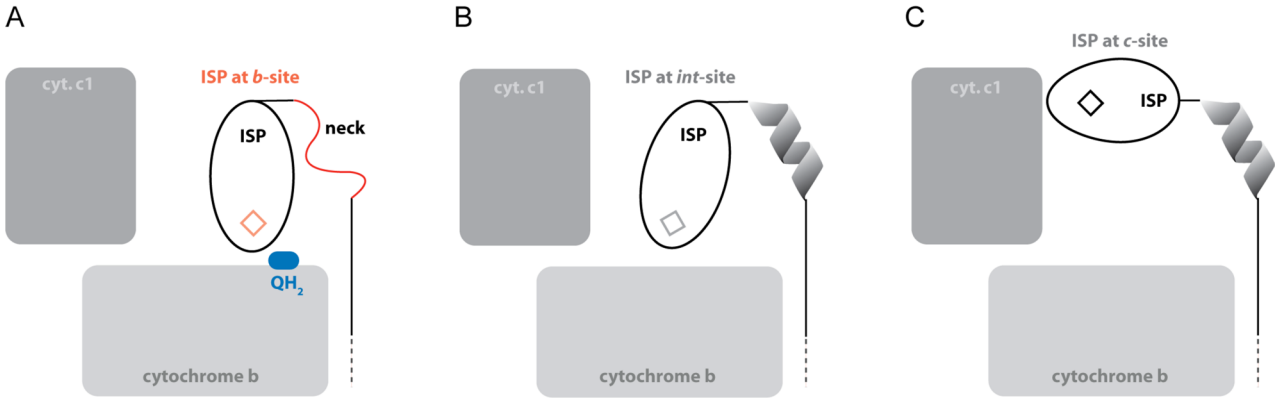

Figure 1. Summary of multiple conformations and sites of the Rieske protein (ISP) in the cytochrome $bc_{(1)}$ complex as reviewed in ref 16. (A) The ISP with a flexible neck (red) and an oxidized cluster (orange diamond) binds at the *b*-site near cytochrome *b* and hydroquinone (QH_2, blue), poised to donate an electron and proton to the ISP.[12] (B) Following the transfer of an electron and proton to the ISP (reduced cluster colored gray), the neck adopts a helical conformation (*int*-site).[15] (C) ISP moves to the *c*-site ready to donate an electron to cytochrome c_1 and a proton to the extracellular space.[15]

becomes helical[15] (Figure 1B). The neck domain remains helical when the ISP is in the *c*-site[15] (Figure 1C). Two types of redox-state-dependent conformational changes have been proposed: a conformational change in the neck domain and a conformational change in the head domain (not emphasized in Figure 1) of the Rieske protein.

In model 2, an alternative mechanism involving passive diffusion between the two sites has been proposed.[8,18,19] This diffusion model decouples the relationship between conformation and function and predicts that ligand binding and redox-state changes are not the primary driving forces behind the movement of the Rieske protein.

We have used NMR spectroscopy to monitor redox-state-dependent and ligand-dependent conformational changes in *Tt*Rp. The conformational change models[1,2,13,15,16] predict a large conformational change originating from redox-state change and/or ligand binding. By monitoring NMR chemical shifts and NOE values as a function of the redox and ligation states, we should be able to identify the location and characteristics of the conformational changes. Because our preliminary studies showed large chemical shift perturbations around Gly169 and Pro170, we proposed that the conformational exchange might originate from the *cis*−*trans* isomerization of the peptidyl−prolyl peptide bond. To test the hypothesis, we prepared a sample of the truncated form of the Rieske protein (trunc-*Tt*Rp) lacking the membrane anchor and incorporating ^{13}C- and ^{15}N-labeled proline and ^{13}C-labeled glycine ([U-^{13}C,^{15}N-Pro][^{13}C-Gly]-trunc-*Tt*Rp). After collecting carbon chemical shifts and proton NOESY spectra under different conditions, we used criteria from the literature[20,21] to determine the likelihood of the Gly169−Pro170 peptide bond being *cis* or *trans* (see Materials and Methods and Supporting Information for details). We detected small conformational changes but found no evidence of the large conformational changes predicted by model 1.[1,12−14] Thus, our results appear to be more consistent with the diffusion model (model 2).[8,18,19]

MATERIALS AND METHODS

Chemicals, Bacterial Strains, and Vectors. [99% ^{15}N]H_4Cl, [99% U-^{13}C]-D-glucose, 99% D_2O, and sodium 2,2-dimethyl-2-silapentane-5-sulfonate (DSS) were purchased from Cambridge Isotope Laboratories (Andover, MA). Unlabeled amino acids, BME vitamins, redox reagents, and the corresponding antibiotics were purchased from Sigma-Aldrich (St. Louis, MO). Isopropyl *β*-D-thiogalactoside (IPTG) was purchased from LabScientific (Livingston, NJ). Dodecylphosphocholine (DPC) was purchased from Avanti Polar Lipids (Alabaster, AL). *Escherichia coli* strain BL21(DE3)pLysS and the *λ*-(DE3) lysogenization kit were purchased from Novagen (Madison, WI). Expression vector pET17b carrying cDNA encoding a truncated soluble domain of *Tt*Rp from *T. thermophilus* strain HB8 (pET17b/trunc-*Tt*Rp) was provided by J. A. Fee (The Scripps Research Institute, La Jolla, CA). Expression vector pET22b carrying cDNA encoding a full-length *Tt*Rp from *T. thermophilus* strain HB27 (pET22b/*Tt*Rp) was provided by B. Ludwig (Biozentrum der Universität Frankfurt, Frankfurt, Germany). *E. coli* strain CAG18447 (with proline deficiency) was purchased from the Coli Genetic Stock Center (Yale University, New Haven, CT). Differences between the two strains are summarized in the Supporting Information.

Protein Expression and Labeling. [U-^{15}N]-trunc-*Tt*Rp and [U-^{13}C,^{15}N]-trunc-*Tt*Rp were produced from BL21(DE3)-pLysS cells containing pET17b/trunc-*Tt*Rp grown in M9 medium containing 1 g/L $^{15}NH_4Cl$ as described previously[3] but with modifications: 50 mg/L (w/v) $FeCl_3$ and 1% (v/v) BME vitamins were added to the growth medium. For ^{13}C labeling, [U-^{13}C]glucose was added in two aliquots with 2 g/L added at the beginning and 2 g/L added when the OD_{600} reached 2.5 (immediately after IPTG induction).

[U-^{13}C,^{15}N-Pro][^{13}C-Gly]-trunc-*Tt*Rp, [^{13}C-Gly]-trunc-*Tt*Rp, and [^{15}N-Gly]-trunc-*Tt*Rp were produced from CAG18447(DE3) cells containing pET17b grown in a rich, synthetic medium as described previously,[22] with the modification that 50% of the amino acids, including the selectively labeled amino acids, were added initially and the remaining 50% of the amino acids were added with IPTG. Strain CAG18447(DE3) was derived from strain CAG18447 by using the standard protocol with a lysogenization kit (Novagen).

[U-^{15}N]-*Tt*Rp and [U-^{13}C,^{15}N]-*Tt*Rp were produced by BL21(DE3)pLysS cells containing pET22b/*Tt*Rp grown in a manner similar to that of [U-^{15}N]-trunc-*Tt*Rp, except that the cells were grown initially in 2 L of LB medium to a high cell density (total OD of ∼6 if pooled into 1 L) before the transfer to the M9 medium. The yield from this medium was ∼1 mg/L

dx.doi.org/10.1021/bi400296c | *Biochemistry* 2013, 52, 2862−2873

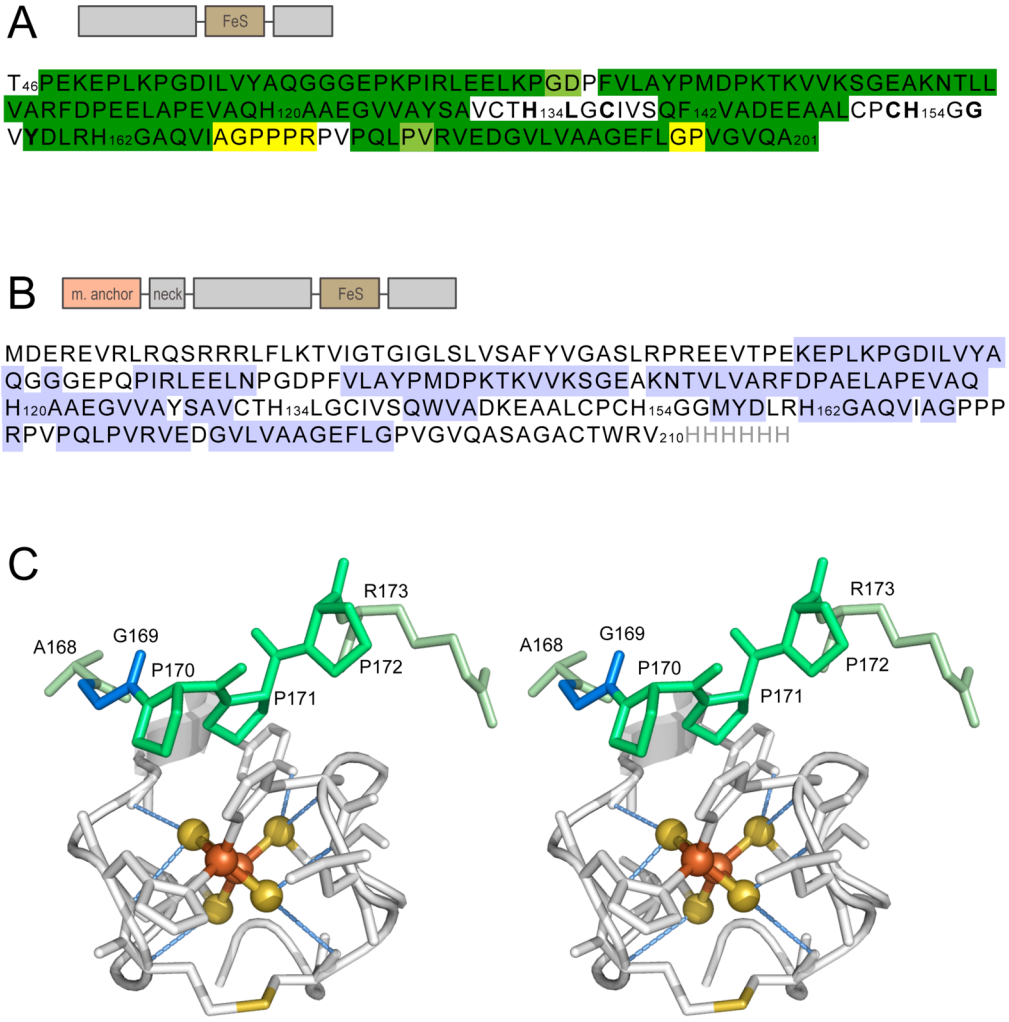

Figure 2. Rieske protein from *T. thermophilus* studied here. (A) Primary sequence of the truncated, water-soluble fragment of the Rieske protein (trunc-*Tt*Rp) used here and in previous crystallographic[3] and NMR studies. The construct[30,32] was truncated to remove the N-terminal transmembrane region (residues 1−45) and nine C-terminal residues (202−210); in addition, it contained the point mutation W142F. The proline loop is highlighted in yellow as is the second GP sequence. Residues highlighted in green are other residues whose NMR assignments were determined in both the oxidized and reduced forms of the protein. (B) Primary sequence of the full-length version of the Rieske protein (*Tt*Rp) (see the Supporting Information for details). Highlighted in blue are residues with assigned NMR signals. The protein contained a C-terminal His_6 tag used for protein purification (light gray). (C) Wall-eyed stereoscopic view of the Fe−S cluster of trunc-*Tt*Rp and the surrounding amino acid residues from the X-ray crystal structure.[3] The proline loop is highlighted. Prolines are colored dark green; G169 is colored blue, and A168 and R173 are colored light green. Blue dashed lines represent hydrogen bonds to the cluster. The G169−P170 peptide bond is modeled as *trans*.

of culture; 0.2−2% DPC and 1 mM DTT were required throughout the purification process.

NMR Sample Preparation. Amicon centrifuge concentrators (Millipore, Billerica, MA) were used for protein concentration and for buffer exchanges following protein purification. The standard NMR buffers were 50 mM Tris and 100 mM NaCl in 9% D_2O at pH 7.5 with 0.2% DPC for *Tt*Rp, 50 mM Tris and 100 mM NaCl at pH 7.4, or a triple buffer consisting of 20 mM Tris, 20 mM phosphate, and 20 mM borate at pH 8.5 for trunc-*Tt*Rp. Tris was omitted from the buffers of samples used to collect NOE data; 2% DPC was required for the studies of binding of ligands to *Tt*Rp. Sodium dithionite or sodium dithiothreitol (for only *Tt*Rp) was used as a reducing agent; ferricyanide was used as the oxidizing agent. NMR samples contained DSS as the internal chemical shift standard. Shigemi (Shigemi, Inc., Allison Park, PA) susceptibility-matched NMR tubes were used for NMR samples containing oxidized Rieske protein. NMR samples containing reduced Rieske protein were prepared in an anaerobic chamber and transferred to NMR tubes sealed by a J. Young valve (Wilmad, Vineland, NJ). The pH meter was calibrated before readings were taken.

NMR Spectroscopy. The temperature of samples of trunc-*Tt*Rp used for HSQC experiments was held at 298 K. The temperature of samples containing *Tt*Rp was held at 298 or 313 K. The redox state of the Rieske protein was controlled by adding oxidizing or reducing agents, and the redox state was determined on the basis of the pattern of one-dimensional ^1H NMR hyperfine shifts.

Conventional triple-resonance data sets, including ^{15}N HSQC, ^{13}C HSQC, HNCACB, CBCACONH, CCONH, HAHBCONH, HCCONH, and NOESY, were collected for trunc-*Tt*Rp and used in determining spectral assignments at given temperatures. ^{15}N HSQC, HNCA, and CACONH data sets were collected for *Tt*Rp.

dx.doi.org/10.1021/bi400296c | *Biochemistry* 2013, 52, 2862−2873

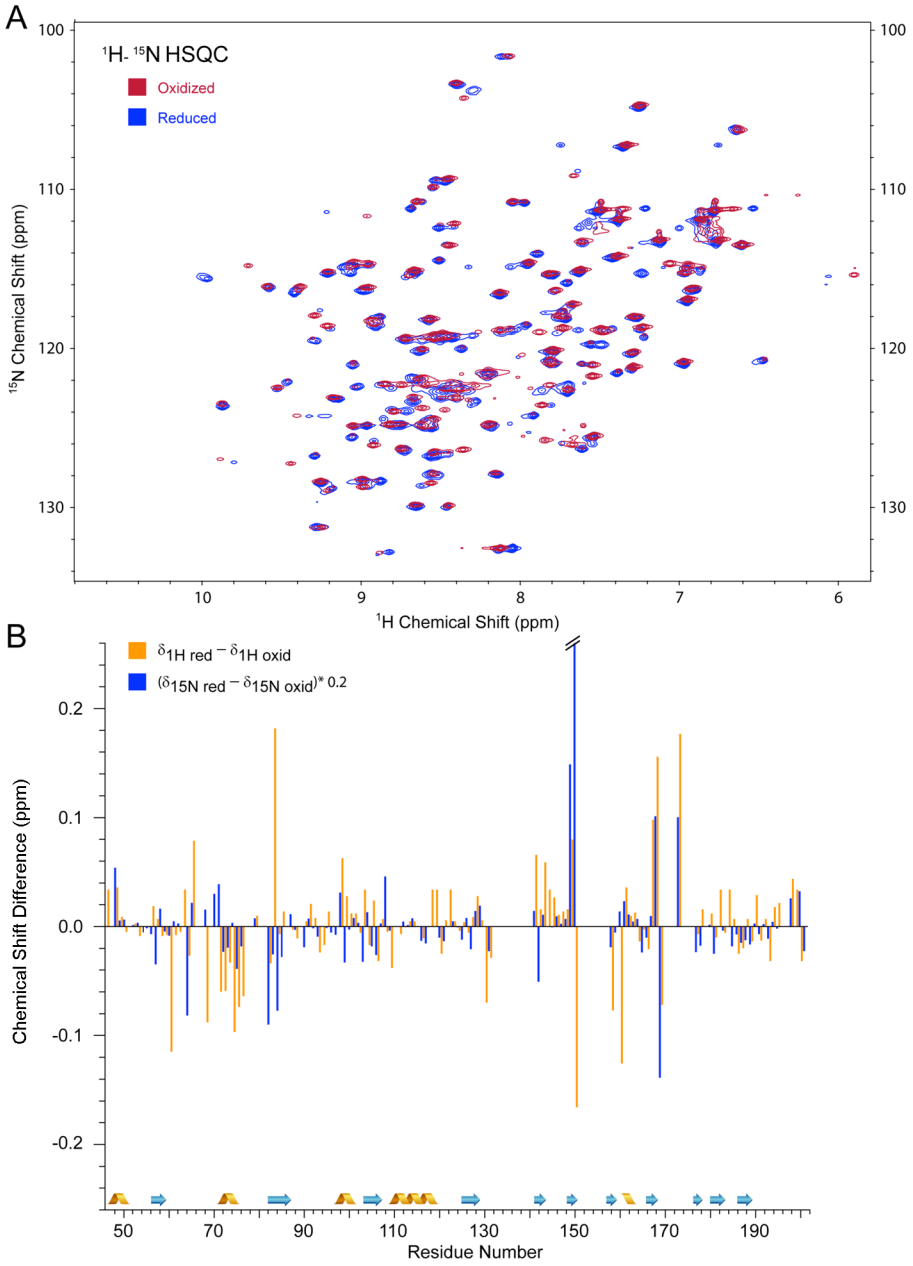

Figure 3. Redox-state-dependent chemical shifts of trunc-*Tt*Rp. (A) Overlaid ^{1}H−^{15}N HSQC spectra of (red) oxidized and (blue) reduced [U-^{13}C,^{15}N]-trunc-*Tt*Rp. The sample conditions were ∼8 mM protein at pH 8.5 and 298 K. (B) Differences in the chemical shifts of backbone amide groups of oxidized and reduced trunc-*Tt*Rp plotted as a function of residue number: (orange) $\Delta\delta^{1}H = \delta^{1}H_{red} - \delta^{1}H_{oxid}$, and (blue) $\Delta\delta^{15}N = \delta^{15}N_{red} - \delta^{15}N_{oxid}$. Very large values were truncated. Secondary structural elements derived from the X-ray crystal structure[3] are indicated at the bottom.

NMR Data Processing and Analysis. Proton chemical shifts were referenced relative to internal DSS (taken as 0 ppm); carbon and nitrogen spectra were referenced indirectly by the canonical ratios.[23] All spectra were processed by XWIN-NMR or Topspin (Bruker) with exponential line broadening. COSY spectra were apodized by applying a Gaussian window function. SPARKY[24] was used for peak picking.

Criteria for Distinguishing the *cis* and *trans* Configurations. Xaa$_{i-1}$-Pro$_i$ sequences in the *cis* configuration typically have prolyl $^{13}C^{\gamma}$ chemical shifts of 24.4 ± 0.7 ppm and $^{13}C^{\beta}$ chemical shifts of 33.8 ± 1.2 ppm with a $\delta(^{13}C^{\beta}) - \delta(^{13}C^{\gamma})$ chemical shift difference of 9.64 ± 1.27 ppm. In addition for *cis* peptide bonds, a NOESY cross-peak is expected between $^{1}H^{\alpha}_{i-1}$ and $^{1}H^{\alpha}_{i}$. Xaa$_{i-1}$-Pro$_i$ sequences in the *trans* configuration typically have prolyl $^{13}C^{\gamma}$ chemical shifts of 27.4 ± 0.9 ppm and $^{13}C^{\beta}$ chemical shifts of 31.8 ± 1.0 ppm with a $\delta(^{13}C^{\beta}) - \delta(^{13}C^{\gamma})$ chemical shift difference of 4.51 ± 1.17 ppm. In addition, for *trans* peptide bonds, a NOESY cross-peak is expected between $^{1}H^{\alpha}_{i-1}$ and $^{1}H^{\delta}_{i}$.[20,21] We also made use of the Promega software program that provides a probabilistic analysis of the configuration of a peptidyl−prolyl peptide bond on the basis of the local sequence and experimental NMR chemical shifts.[20]

RESULTS

NMR Resonance Assignments. Of the 156 residues of trunc-*Tt*Rp, we were able to assign NMR signals to 134 residues in the reduced state and 130 residues in the oxidized state (Figure 2A) by standard double- and triple-resonance

dx.doi.org/10.1021/bi400296c | *Biochemistry* 2013, 52, 2862−2873

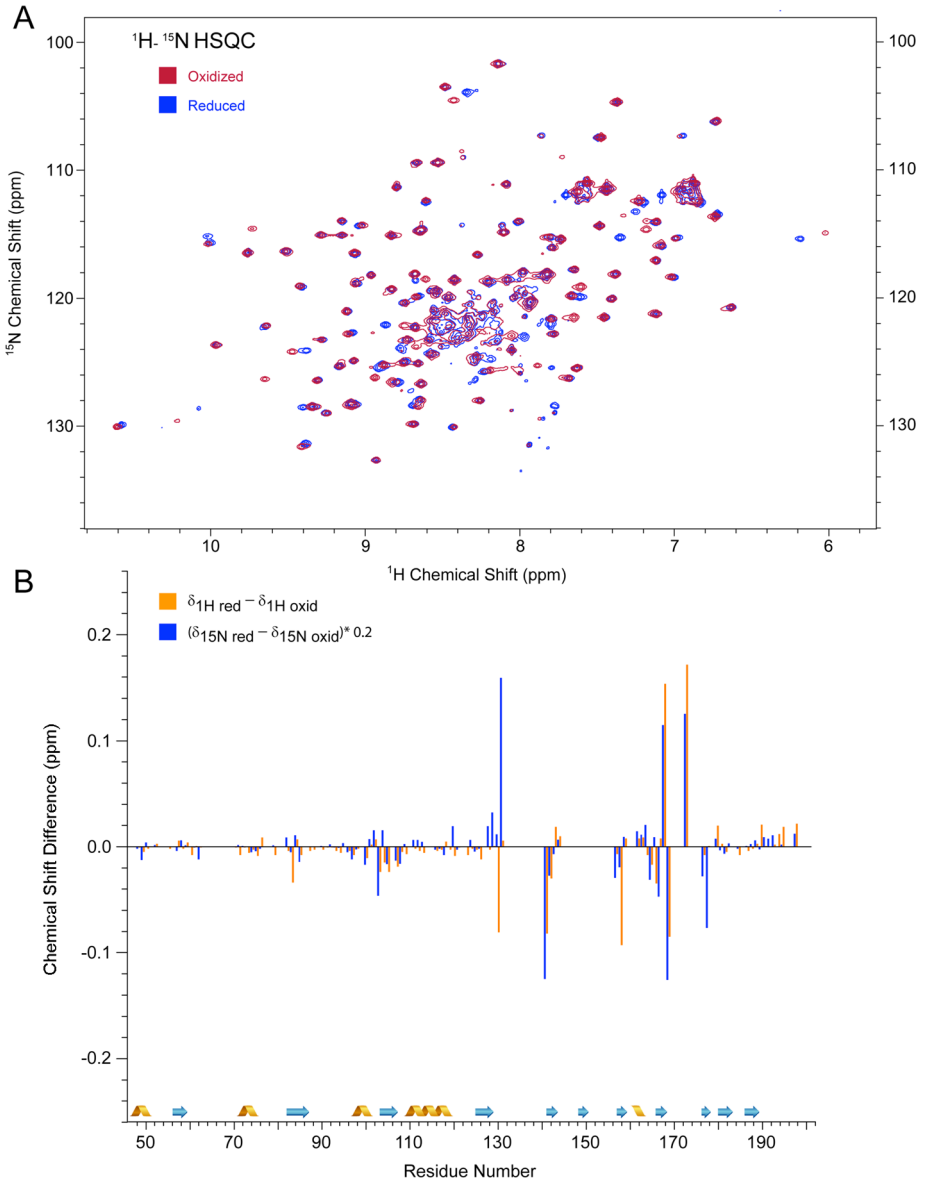

Figure 4. Redox-state-dependent chemical shifts of *Tt*Rp. (A) Overlaid ^{1}H−^{15}N HSQC spectra of (red) oxidized and (blue) reduced [U-^{13}C,^{15}N]-*Tt*Rp. The sample conditions were 0.1 mM protein at pH 7.5 in 0.2% DPC micelles. NMR spectra were recorded at 313 K. (B) Differences in the chemical shifts of backbone amide groups of oxidized and reduced *Tt*Rp plotted as a function of residue number: (orange) $\Delta\delta^{1}H = \delta^{1}H_{red} - \delta^{1}H_{oxid}$, and (blue) $\Delta\delta^{15}N = \delta^{15}N_{red} - \delta^{15}N_{oxid}$. Secondary structural elements derived from the X-ray crystal structure[3] are indicated at the bottom.

methods. Apart from the 18 residues belonging to the two loops (131−140 and 150−157) that surround the Fe−S cluster, which we did not expect to be able to assign because of the paramagnetism of the cluster, the assignments account for more than 94% of the residues of trunc-*Tt*Rp. We then extended these assignments to the full-length Rieske protein (*Tt*Rp) by comparison to triple-resonance data. We used residue selective and reverse labeling methods (see Figure S1 of the Supporting Information) to extend and verify the assignments to a level of 55% (Figure 2B). Paramagnetic optimized NMR pulse sequences[25,26] were required for the observation of signals from residues near the Fe−S cluster in the reduced protein.

Redox-State-Dependent NMR Spectral Changes. We collected ^{1}H−^{15}N HSQC NMR spectra of oxidized and reduced trunc-*Tt*Rp (Figure 3A) and compared the chemical shift differences of the ^{1}H and ^{15}N signals as a function of residue number (Figure 3B). The largest chemical shift changes mapped onto residues 76−78 (strand), 149 and 150 (strand), and 169−173 (loop). We conducted a similar analysis of full-length Rieske protein (*Tt*Rp) in the presence of 0.2% DPC micelles (Figure 4). In this case, the largest redox-state-dependent chemical shift differences mapped to residues 130, 140, 168, 170, and 178. Residues Gly169, Pro170, Pro171, Pro172, and R173 exhibited large redox-state-dependent chemical shift differences in both *Tt*Rp and trunc-*Tt*Rp. We refer to these residues as the proline loop. On the basis of the X-ray structure (see Figure 2C), these residues have an average Fe−S distance of ∼6 Å.

Configuration of the Gly169−Pro170 Peptide Bond in the Reduced Rieske Protein. We collected data from multiple spectra of reduced trunc-*Tt*Rp and focused on signals from residues around Gly169 and Pro170 (Figure 5A). A set of weak NOESY cross-peaks (Figure 5B−D) confirmed the assignments. We collected NOESY data at different mixing

dx.doi.org/10.1021/bi400296c | *Biochemistry* 2013, 52, 2862−2873

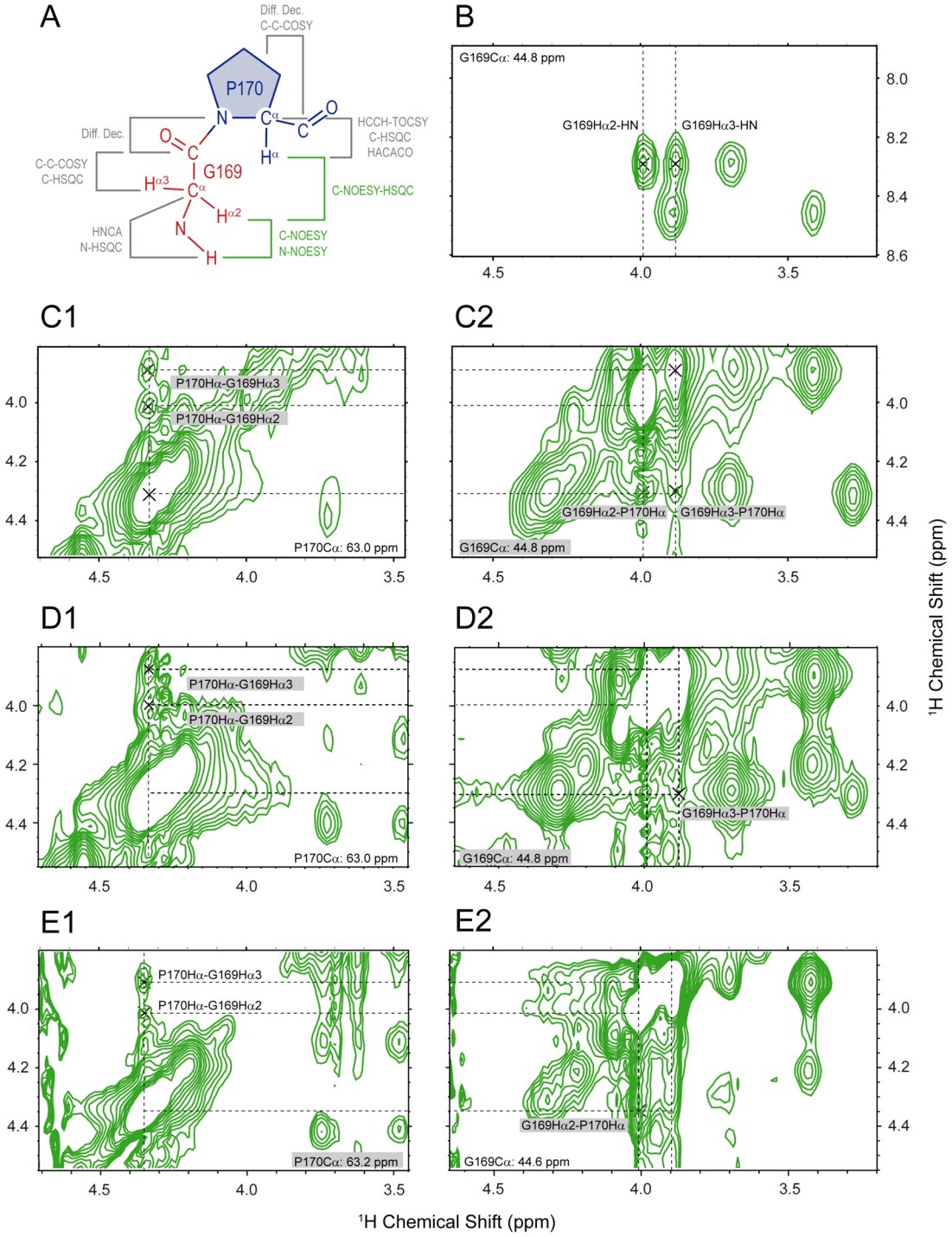

Figure 5. Evidence showing that the Gly169−Pro170 peptide bond is *cis* when the protein is reduced. (A) Diagram showing a *cis* Gly-Pro dipeptide. Colored gray are the experiments used to identify signals from key atoms. Colored green are the nuclear Overhauser effect (NOE) experiments used to identify short distances between ^{1}H atoms. (B−D) Planes from three-dimensional proton−carbon−proton NOESY-HSQC spectra of freshly reduced 3 mM [U- ^{13}C,^{15}N-Pro][U-^{13}C-Gly]-trunc-*Tt*Rp acquired at pH 7.5 without Tris buffer for higher sensitivity and 298 K with NOESY mixing times of 23 and 45 ms and repeated at pH 8.0 with a NOESY mixing time of 45 ms. (B) Plane from an experiment collected with a τ_m of 23 ms. The sample was at pH 7.5 and 298 K. Starting from the Gly169 $^{1}H^{N}$, we extended the assignments (by following the dashed lines between panels B and C2) to Gly169 $^{1}H^{\alpha}$. (C1) Plane containing the signal from Pro170 $^{13}C^{\alpha}$ (at 63.0 ppm). Two NOE cross-peaks were observed: Pro170 $^{1}H^{\alpha}$−Gly169 $^{1}H^{\alpha 2}$ and Pro170 $^{1}H^{\alpha}$−Gly169 $^{1}H^{\alpha 3}$. The mixing time was 23 ms, and the sample was at pH 7.5 and 298 K. (C2) Plane containing the signal from Gly169 $^{13}C^{\alpha}$ (at 44.8 ppm). Again, two NOEs were observed: Gly169 $^{1}H^{\alpha 2}$−Pro170 $^{1}H^{\alpha}$ and Gly169 $^{1}H^{\alpha 3}$−Pro170 $^{1}H^{\alpha}$. The mixing time was 23 ms, and the sample was at pH 7.5 and 298 K. (D1) Same sample and spectral plane as shown in panel C1 except that the mixing time was 45 ms. (D2) Same sample and spectral plane as shown in panel C2 except that the mixing time was 45 ms. (E1) Same spectral plane as in panels C1 and D2, except that the mixing time was 45 ms and the sample pH was 8.0. (E2) Same spectral plane as in panels C1 and D2, except that the mixing time was 45 ms and the sample pH was 8.0.

dx.doi.org/10.1021/bi400296c | *Biochemistry* 2013, 52, 2862−2873

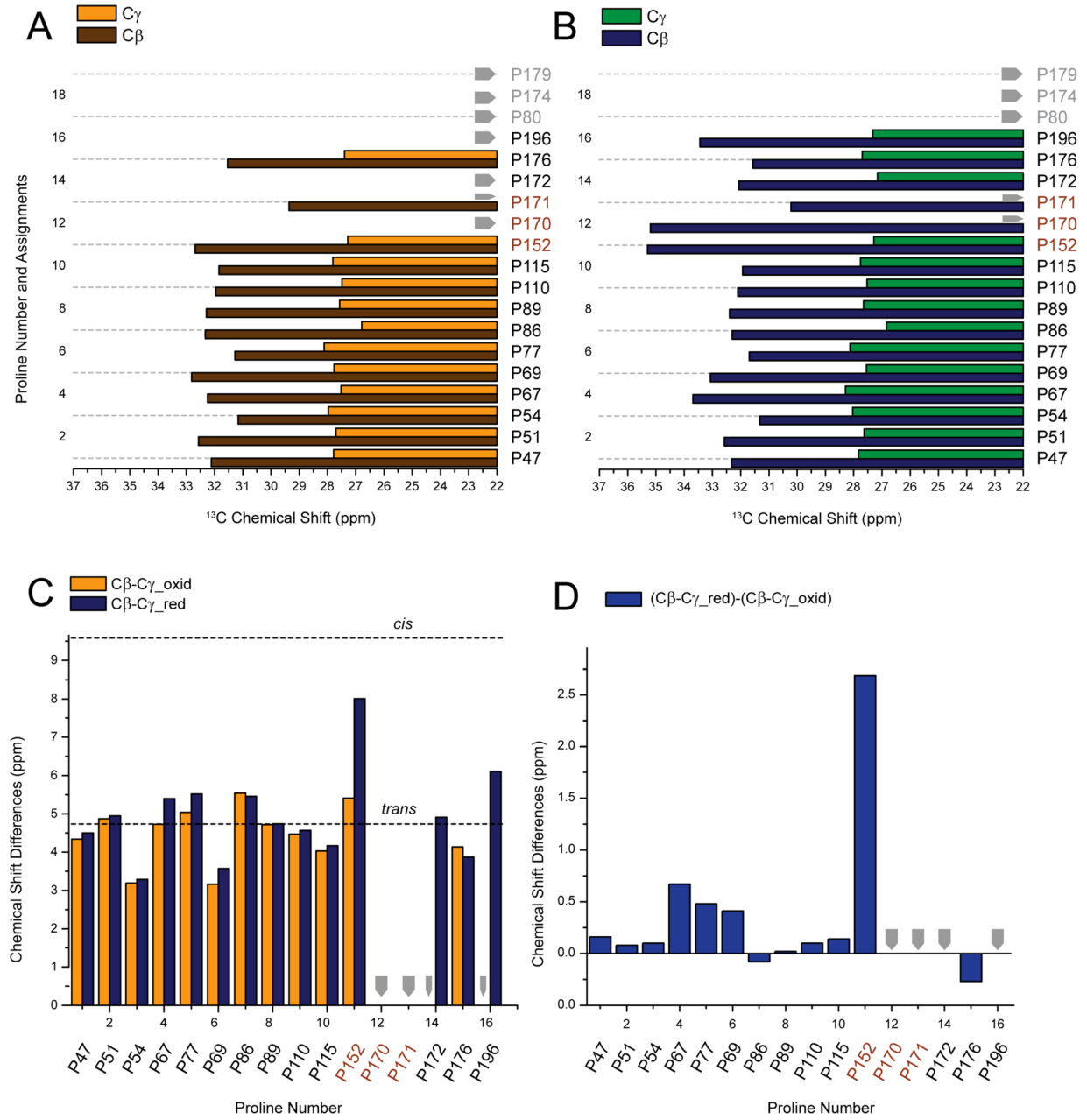

Figure 6. Redox-state-dependent proline chemical shift changes of trunc-*Tt*Rp. (A) Proline C^{β} and C^{γ} chemical shifts of 3 mM [U-^{13}C,^{15}N-Pro][^{13}C-Gly]-trunc-*Tt*Rp at pH 7.4 and 298 K in the oxidized state: (brown bars) $^{13}C^{\gamma}$ and (orange bars) $^{13}C^{\beta}$. Signals from three prolyl residues (P80, P174, and P179) were not assigned in either redox state and were omitted (C and D) for the sake of clarity; these three are far from the iron−sulfur center. Three prolyl residues that are close to the iron−sulfur center exhibited paramagnetic broadening (P152, P170, and P171). Gray arrows denote atoms whose signals were missing or unassigned. (B) Carbon chemical shifts in the reduced state. (C) Chemical shift differences ($\delta^{13}C^{\beta} - \delta^{13}C^{\gamma}$) (blue) in the reduced state and (orange) in the oxidized state. The dashed lines marked *trans* and *cis* indicate average chemical differences for these respective peptide bond configurations.[21] (D) Difference between the chemical shift differences $[(\delta^{13}C^{\beta} - \delta^{13}C^{\gamma})_{reduced} - (\delta^{13}C^{\beta} - \delta^{13}C^{\gamma})_{oxidized}]$ in reduced and oxidized trunc-*Tt*Rp.

times (τ_m), temperatures, and pH values: τ_m = 23 ms at 298 K and pH 7.5 (Figure 5C); τ_m = 45 ms at 298 K and pH 7.5 (Figure 5D); τ_m = 45 ms at 298 K and pH 8.0 (Figure 5E); and τ_m = 45 ms at pH 8.0 and 300 K (data not shown). Cross-peaks were observed under all these conditions, indicative of a *cis* configuration for the G169−P170 peptide bond.

Analysis of Prolyl Residue Chemical Shifts. In addition to NOEs, prolyl $^{13}C^{\beta}$ and $^{13}C^{\gamma}$ chemical shifts are helpful for determining the configuration of the peptidyl−prolyl peptide bond, and the chemical shift difference $\delta(^{13}C^{\beta}) - \delta(^{13}C^{\gamma})$ provides an even better diagnostic.[21] Trunc-*Tt*Rp contains 19 prolyl residues. With oxidized *Tt*Rp (Figure 6A), we determined both the $^{13}C^{\beta}$ and $^{13}C^{\gamma}$ chemical shifts for 12 prolyl residues (P47, P51, P54, P67, P69, P77, P86, P89, P110, P115, P152, and P176) and only $^{13}C^{\beta}$ for one (P171). With reduced *Tt*Rp (Figure 6B), we determined both $^{13}C^{\beta}$ and $^{13}C^{\gamma}$ chemical shifts for 14 prolyl residues (P47, P51, P54, P67, P69, P77, P86, P89, P110, P115, P152, P172, P176, and P196) and only $^{13}C^{\beta}$ for two (P170 and P171). In the oxidized state, the prolyl $^{13}C^{\beta}$ and $^{13}C^{\gamma}$ chemical shifts of trunc-*Tt*Rp (Figure 6A)

dx.doi.org/10.1021/bi400296c | *Biochemistry* 2013, 52, 2862−2873

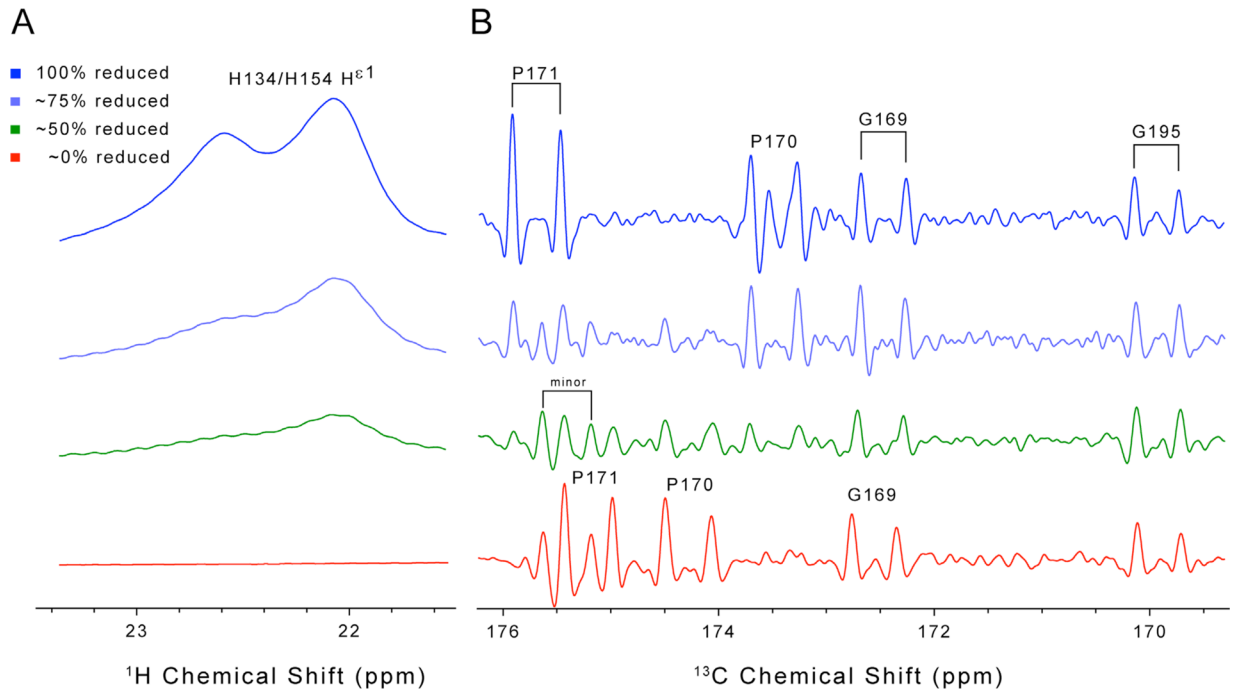

Figure 7. Redox-state-dependent conformational changes observed in NMR spectra of trunc-*Tt*Rp. (A) Proton SuperWEFT and (B) $^{13}C-[^{15}N]$ difference decoupling spectra of 6.5 mM [U-^{13}C,^{15}N-Pro][^{13}C-Gly]-trunc-*Tt*Rp collected at pH 7.4 and 298 K. The ^{1}H hyperfine-shifted signals around 22−23 ppm in panel A, which are observed only in the reduced protein and serve as a monitor of the redox state, were assigned to His134/154 $^{1}H^{\varepsilon 1}$. The $^{13}C'$ signals assigned to P171 and P170 in panel A exhibited large, redox-state-dependent chemical shift changes; the $^{13}C'$ signal assigned to G169 exhibited a smaller change, and the $^{13}C'$ signal assigned to G195 exhibited no change.

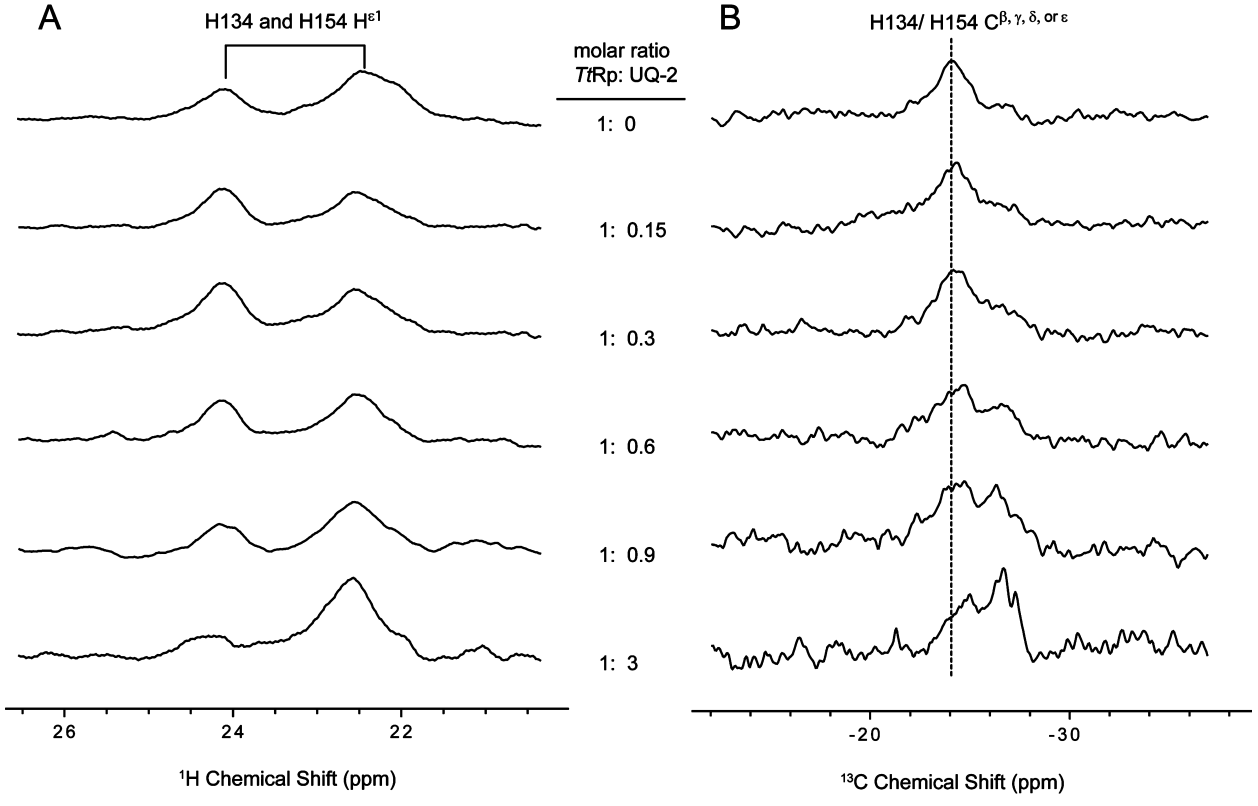

Figure 8. Effect of added UQ-2 on hyperfine signals from reduced *Tt*Rp in the presence of 2% DPC micelles. The NMR sample contained 0.9 mM [U-^{13}C,^{15}N]-*Tt*Rp at pH 7.5; data were collected at 313 K. (A) His $^{1}H^{\varepsilon 1}$ signals from the two iron-ligating histidines. (B) Side chain carbon signals from the iron-ligating histidines.

are all in the range expected for the *trans* configuration as are the $\delta(^{13}C^{\beta}) - \delta(^{13}C^{\gamma})$ values (Figure 6C). In the reduced state, the $^{13}C^{\beta}$ chemical shifts of P152 and P170 (Figure 6B) are indicative of the *cis* configuration, and the $\delta(^{13}C^{\beta}) - \delta(^{13}C^{\gamma})$

dx.doi.org/10.1021/bi400296c | *Biochemistry* 2013, 52, 2862−2873

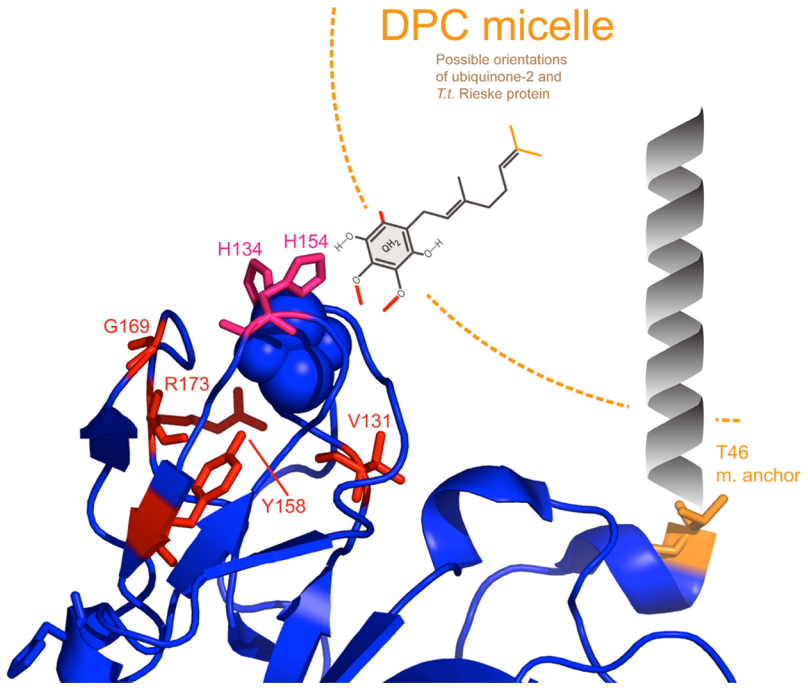

Figure 9. Model depicting the putative interaction between oxidized *Tt*Rp and reduced hydroubiquinone-2 (UQ-2). The protein structure shown is adapted from the X-ray crystal structure of trunc-*Tt*Rp.[3] The N-terminal residue of that structure (T46) is colored orange. The neck domain and the membrane anchor domain (not modeled in the X-ray structure) are colored gray. Residues that exhibited sizable chemical shift changes upon the addition of UQ-2 are colored red. Residues of the Rieske protein whose hyperfine signals exhibited changes upon the addition of UQ-2 are colored magenta. NMR signals from the terminal methyl protons of UQ-2 (red) exhibited changes in the presence of the protein. The model proposes specific binding with a possible hydrogen bond between the hydroxyl group of UQ-2 and the deprotonated ring nitrogen of H154.

value for P152 confirms the *cis* configuration. Although we were unable to determine the chemical shift difference for P170 in reduced trunc-*Tt*Rp, because the signal from its $^{13}C^{\gamma}$ was not observed, Promega[20] analysis of the observed chemical shifts yielded a high (normalized) probability (94%) for a *cis* G169−P170 peptide bond. Moreover, the NOE results (Figure 5) provided unequivocal evidence of a *cis* peptide bond. Further information about the redox-state dependence of prolyl chemical shifts is given in Figure S2 of the Supporting Information.

Hyperfine Signals from Residues in the Proline Loop. Several atoms from residues in the proline loop are close enough to the iron−sulfur cluster to experience severe broadening. We used NMR pulse sequences optimized for hyperfine signals to determine their chemical shifts in fully reduced and fully oxidized Rieske protein. To determine the fraction reduced, we measured the intensity of the hyperfine ^{1}H NMR signals arising from the histidine residues that ligate the cluster, which are observed only when the Rieske protein is reduced (Figure 7A). We then correlated the fraction reduced with spectral changes in signals assigned to the carbonyl carbons of G169, P170, P171, and G195 (Figure 7B). G195, which is not part of the proline loop, exhibited no chemical shift change with change in redox state. The chemical shift of G169 $^{13}C'$ changed by only ∼0.1 ppm between the oxidized and reduced states, with the signal changing continuously as indicative of fast exchange on the chemical shift time scale. By contrast, the $^{13}C'$ signals from P170 and P171 changed by ∼1.0 ppm between oxidation states and exhibited slow exchange.

Spectral Changes upon Binding of Ubiquinone. Members of the Rieske protein family bind different quinones: eukaryotic Rieske proteins bind ubiquinone-*n*, and bacterial Rieske proteins bind menaquinone-*n* (Figure S3 of the Supporting Information). Quinones consist of various numbers (*n*) of isoprene units as membrane anchors. Our attempts to observe interactions between trunc-*Tt*Rp and quinones were unsuccessful; however, we found evidence from NMR that the full-length protein *Tt*Rp in the presence of 2% DPC bound hydroubiquinone-2 (UQ-2). The longer chain hydromenaquinone-4 was not soluble under the same conditions (see the Supporting Information for details).

We collected NMR spectra of mixtures of 0.1 mM reduced *Tt*Rp and 1.5 mM UQ-2 at different molar ratios. NMR signals from more than five residues showed perturbations as a function of the *Tt*Rp:UQ-2 molar ratio (1:0, 1:0.33, 1:1, and 1:2) (Figure S4A of the Supporting Information). At a molar ratio of 1:0, *Tt*Rp was ligand free. At ratios of 1:1 and 1:2, the major population likely was the *Tt*Rp−UQ-2 complex. At a molar ratio of 1:0.33, separate signals were observed from free *Tt*Rp and the *Tt*Rp−UQ-2 complex. Interestingly, the UQ-2 linewidth did not seem to change upon binding.

To determine whether UQ-2 was binding near the iron−sulfur cluster, we monitored hyperfine ^{1}H and ^{13}C signals from the two histidine ligands of reduced *Tt*Rp in the presence of 2% DPC as a function of added UQ-2 (Figure 8). The intensity of the hyperfine ^{1}H signal at 24.2 ppm decreased with increasing UQ-2 concentration, whereas the intensity of the hyperfine signal at 22.5 ppm remained the same (Figure 8A). The hyperfine ^{13}C signal at −24.5 ppm assigned to a histidine side chain carbon lost intensity with an increasing UQ-2 concentration, and a new signal grew in at approximately −27 ppm (Figure 8B). $^{1}H-^{15}N$ HSQC spectra acquired as a function of UQ-2 concentration (data not shown) exhibited changes in signals from residues around the iron−sulfur cluster

dx.doi.org/10.1021/bi400296c | *Biochemistry* 2013, 52, 2862−2873

(V131, Y158, G169, and R173). Signals from UQ-2 also were found to change upon complex formation. The 2′-, 3′-, and 5′-methyl ^{13}C signals exhibited changes attributed to hyperfine interaction with the iron−sulfur cluster (Figure S5 of the Supporting Information). The model depicted in Figure 9 summarizes information from NMR on the UQ-2-Rieske protein interaction.

DISCUSSION

Redox-State-Dependent Peptide Bond Isomerizations. Data presented here provide information about the configuration of 13 of the 19 peptidyl−prolyl peptide bonds as a function of oxidation state. All 13 were found to be *trans* in oxidized trunc-*Tt*Rp, and two of these (P152 and P170) became *cis* in reduced trunc-*Tt*Rp. P170 is in the proline loop that lies close to the iron−sulfur cluster, and P152 also is close enough to the cluster to experience hyperfine effects. The position of the Pro152 $^{13}C'$ resonance exhibited a temperature-dependent shift between 298 and 313 K indicative of a Fermi-contact contribution (data not shown). Thus, the likely mechanism for both isomerizations is differential interaction of the *cis* and *trans* configurations with the oxidized and reduced cluster. Because of the close agreement between the chemical shifts of these regions in spectra of trunc-*Tt*Rp and *Tt*Rp (Figures 3B and 4B), these redox-state-dependent changes in the configuration of the P152 and P170 peptide bonds also appear to occur in full-length Rieske protein bound to micelles. Because the proline loop is highly conserved (Figure S6 of the Supporting Information), it may play an important role in the differential interaction of the Rieske protein with its two protein partners.

Iwata et al. have published low-resolution (3.0 Å) X-ray crystal structures of the oxidized bovine cytochrome $bc_{(1)}$ complex with and without bound inhibitors;[15] their structures indicated site-dependent structural changes in the Rieske protein. Their structural models showed *P*175 (corresponding to P170 in *Tt*Rp) in the *trans* configuration in *c*-site and in the *cis* configuration in the *int*-site [see Figure S6 of the Supporting Information for sequence alignment between bovine Rieske protein and *Tt*Rp; the blue arrow points to P170 (*P*175)]. This result is in agreement with the NMR evidence presented here for the redox-state-dependent configuration of P170.

Comparison of Solution and Crystal Structures. We measured residual dipolar couplings (RDCs) as a means of comparing the solution structure with the crystal structure of oxidized trunc-*Tt*Rp.[3] Our RDCs from oxidized trunc-*Tt*Rp are consistent with the X-ray crystal structure, whereas those of reduced trunc-*Tt*Rp are not (Figure S7 of the Supporting Information). Solmaz et al.[27] did not observe *cis* peptidyl−prolyl peptide bonds in the residues homologous to Rieske P152 and P170 in the 1.9 Å X-ray structure of the reduced cytochrome $bc_{(1)}$ complex in the presence of the inhibitor stigmatellin. The reason for this discrepancy may be that stigmatellin, which is classified as a P_f inhibitor,[28] "fixes" the conformation of the *b*-site, causing it to lose its mobility. Other reasons could be the low degree of sequence similarity to trunc-*Tt*Rp or contributions from the other protein subunits. In an earlier study,[29] Konkle et al. found that the X-ray structure of oxidized trunc-*Tt*Rp crystallized at low pH (6.0) does not differ much from that crystallized at pH 8.5. We collected $^{1}H-^{15}N$ HSQC spectra of reduced trunc-*Tt*Rp at seven pH values ranging from 5.2 to 8.4 and found only minor chemical shift changes (data not shown), implying that the Rieske protein does not exhibit pH-dependent conformational changes over that range.

Evidence of a Local, Rather Than Global, Redox-State-Dependent Conformational Change. Our $^{1}H-^{15}N$ HSQC results (Figures 2 and 3) suggest that the conformational change is local and minor. This is in agreement with an earlier analysis from $^{13}C^{\alpha}$ and $^{13}C^{\beta}$ chemical shifts,[30] which indicated no change in secondary structure with change in redox state. The neck domain of the Rieske proteins has been reported to undergo a redox-state-dependent conformational change in studies of the cytochrome $bc_{(1)}$ complex.[17] However, our studies of isolated *Tt*Rp gave no indication of such a conformational change. The presence of other subunits may be required for this effect. In summary, we found no evidence supporting large redox-state-dependent conformational changes in the Rieske protein; however, we found evidence that the configurations of the peptidyl−prolyl peptide bonds of P152 and P170 change from *trans* to *cis* upon reducing the protein.

Ubiquinone Binding. Our studies show that reduced *Tt*Rp in the presence of DPC micelles binds UQ-2. At least six *Tt*Rp residues and three sites on UQ-2 showed sizable chemical shift perturbations resulting from the interaction. On the basis of observed hyperfine shifts of *Tt*Rp signals upon binding UQ-2 and the spatial distribution of the *Tt*Rp residues involved, the binding is likely specific. We propose a model for the interaction with a possible hydrogen bond that would provide a pathway for the hyperfine interaction (Figure 9). Because we failed to see an interaction between benzoquinone (in either oxidation state) and trunc-*Tt*Rp, we conclude that the membrane anchors in both the protein and quinone contribute to the binding affinity. UQ-2 binding led to changes in the $^{1}H^{N}$ and ^{15}N chemical shifts of residues V131, Y158, G169, and R173; these changes may indicate that quinone binding induces a local conformational change. These residues are strictly conserved (Y158 and G169), highly conserved (V131), or similar (R173) in sequence alignments (Figure S6 of the Supporting Information). Y158 may be strictly conserved because it hydrogen bonds to the iron−sulfur cluster. The two histidines (H134 and H154) are conserved as cluster ligands. Glycines are known for their flexibility and allowance for a greater range of backbone torsion angles. Prolines are known for their propensity to form loops. The loop containing P152 and P170 appears to form a conserved region for redox-state-dependent and quinone-dependent conformational changes. The redox-state-dependent and ligand-dependent chemical shift changes affecting residues V131, Y158, G169, and R173 are similar (Figures 3B and 4B Figure S4B of the Supporting Information). The native reduced state is in the UQ-2-free conformation, and the oxidized-state conformation resembles the UQ-2-bound form. This appears to imply that a favored interaction between oxidized protein and reduced quinone (Figure 4B and Figure S4B of the Supporting Information).

Electron Transfer Mechanism. Our results show preferential binding between hydroubiquinone and the active site of reduced *Tt*Rp (Figure 9). Hydroubiquinone binding results in local changes in residues around the proline loop but no large conformational change. The local environment of the iron−sulfur cluster is fairly rigid (Figure 2C), with the iron−sulfur cluster fixed by its cysteine and histidine ligands, its hydrogen bond contributors, and a disulfide bridge. The only flexibility seems to be in the proline loop, which undergoes a redox-state-dependent conformational change involving *cis*−*trans* isomerization of the G169−P170 peptide bond. This conformational

dx.doi.org/10.1021/bi400296c | *Biochemistry* 2013, 52, 2862−2873

change and the local flexibility around the proline loop may help the Rieske protein to adapt to different binding pockets in the *b*- and *c*-sites and to facilitate the transfer of an electron to the quinone.

Our results do not support a large ligand-dependent or redox-state-dependent conformational change in the isolated Rieske protein. The large conformational change in the Rieske protein observed by X-ray crystallography[15,16] appears to occur only when cytochrome *b* and/or *c* is present. Our results with *Tt*Rp do not support a large conformational change in the Rieske protein as the driving force for movement of the Rieske protein between the two sites. The contribution made by the proline loop to interactions at the *b*- and *c*-sites is currently unknown, but it appears likely that changes in this loop affect the interactions. Although our results do not exclude the possibility of this conformational change as the driving force in the whole complex, they appear to be more consistent with diffusion-driven movement[8,18,19] of the Rieske protein between the *b*- and *c*-sites.

Our findings are compatible with the following model. In the *b*-site, where the Rieske protein is oxidized and histidine 154 is deprotonated, P152 and P170 adopt the *trans* configuration. After the concerted proton and electron transfer from hydroubiquinone,[30,31] the Rieske protein is reduced, histidine 154 is protonated, and P152 and P170 adopt the *cis* configuration. The conversion to the *cis* configuration might help the Rieske protein dissociate from the *b*-site to reach the *int*-site and/or *c*-site. After reaching the *c*-site, the electron is transferred to cytochrome *c*, and *Tt*Rp reverts to the *trans* state and histidine 154 becomes deprotonated (before binding hydroubiquinone), releasing the proton to the environment to resume the next cycle. The redox-state-dependent and ligand-dependent conformational changes may facilitate binding events in both *b*- and *c*-site pockets to accelerate electron transfer and to prevent short-circuiting.

■ ASSOCIATED CONTENT

Supporting Information

Information regarding strains for protein production, additional NMR assignments, and other ligands tested and eight figures. This material is available free of charge via the Internet at http://pubs.acs.org.

■ AUTHOR INFORMATION

Corresponding Author

*E-mail: markley@nmrfam.wisc.edu. Phone: (608) 263-9349. Fax: (608) 262-3759.

Present Address

K.-L.H.: Institute of Biomedical Sciences, Academia Sinica, Nankang, Taipei 11529, Taiwan.

Author Contributions

K.-L.H. and J.L.M. designed the experiments. K.-L.H., M.T., and K.C. conducted the NMR experiments with advice from W.M.W. K.-L.H. conducted the data analysis and wrote the first draft of the manuscript. All authors approved the final form of the manuscript.

Funding

This work was supported by National Institutes of Health (NIH) Grants R01 GM58667 and U01 GM94622 in collaboration with the National Magnetic Resonance Facility at Madison, which is supported by NIH grants from the National Center for Research Resources (5P41RR002301-27 and RR02301-26S1) and the National Institute for General Medical Sciences (8 P41 GM103399-27).

Notes

The authors declare no competing financial interest.

■ ACKNOWLEDGMENTS

The late James A. Fee (Scripps Research Institute) supplied the plasmid encoding trunc-*Tt*Rp, and Bernd Ludwig (Biozentrum der Universität Frankfurt) provided the plasmid encoding *Tt*Rp. We thank Siok W. Gan (Nanyang Technological University, Singapore) and Ronnie O. Frederick (University of Wisconsin, Madison, WI) for their help with the purification and handling of *Tt*Rp and trunc-*Tt*Rp.

■ ABBREVIATIONS

UQ-2, hydroubiquinone-2; *Tt*Rp, full-length Rieske protein from *T. thermophilus*; trunc-*Tt*Rp, version of *Tt*Rp truncated to remove the N-terminal transmembrane region (residues 1−45) and the nine C-terminal residues (202−210). In addition, it contains the point mutation W142F. This is the version of the protein used in earlier X-ray[3] and NMR[30,32] studies and one other study.[31] Residue names and numbers in normal font refer to the Rieske protein from *T. thermophilus*, and residue names and numbers in italic font refer to the Rieske protein from *Bos tarus*.

■ REFERENCES

(1) Link, T. A. (2001) Fe-S Rieske center. In *Handbook of Metalloproteins* (Albrecht Messerschmidt, R. H., Wieghardt, K., and Poulos, T., Eds.) pp 518−531, Wiley, New York.

(2) Link, T. A. (2001) Cytochrome bc_1 complex. In *Handbook of Metalloproteins* (Albrecht Messerschmidt, R. H., Wieghardt, K., and Poulos, T., Eds.) pp 402−423, Wiley, New York.

(3) Hunsicker-Wang, L. M., Heine, A., Chen, Y., Luna, E. P., Todaro, T., Zhang, Y. M., Williams, P. A., McRee, D. E., Hirst, J., Stout, C. D., and Fee, J. A. (2003) High-resolution structure of the soluble, respiratory-type Rieske protein from *Thermus thermophilus*: Analysis and comparison. *Biochemistry 42*, 7303−7317.

(4) Mooser, D., Maneg, O., Corvey, C., Steiner, T., Malatesta, F., Karas, M., Soulimane, T., and Ludwig, B. (2005) A four-subunit cytochrome $bc_{(1)}$ complex complements the respiratory chain of *Thermus thermophilus*. *Biochim. Biophys. Acta 1708*, 262−274.

(5) Mooser, D., Maneg, O., MacMillan, F., Malatesta, F., Soulimane, T., and Ludwig, B. (2006) The menaquinol-oxidizing cytochrome bc complex from *Thermus thermophilus*: Protein domains and subunits. *Biochim. Biophys. Acta 1757*, 1084−1095.

(6) Nelson, D. L., Cox, M. M., and Lehninger, A. L. (2005) *Lehninger principles of biochemistry*, 4th ed., W. H. Freeman, New York.

(7) Mitchell, P. (1976) Possible molecular mechanisms of the protonmotive function of cytochrome systems. *J. Theor. Biol. 62*, 327−367.

(8) Crofts, A. R., Shinkarev, V. P., Kolling, D. R., and Hong, S. (2003) The modified Q-cycle explains the apparent mismatch between the kinetics of reduction of cytochromes c1 and bH in the bc1 complex. *J. Biol. Chem. 278*, 36191−36201.

(9) Crofts, A. R., Holland, J. T., Victoria, D., Kolling, D. R., Dikanov, S. A., Gilbreth, R., Lhee, S., Kuras, R., and Kuras, M. G. (2008) The Q-cycle reviewed: How well does a monomeric mechanism of the $bc_{(1)}$ complex account for the function of a dimeric complex? *Biochim. Biophys. Acta 1777*, 1001−1019.

(10) Berry, E. A., Guergova-Kuras, M., Huang, L. S., and Crofts, A. R. (2000) Structure and function of cytochrome bc complexes. *Annu. Rev. Biochem. 69*, 1005−1075.

(11) Xiao, K., Yu, L., and Yu, C. A. (2000) Confirmation of the involvement of protein domain movement during the catalytic cycle of the cytochrome bc1 complex by the formation of an intersubunit

disulfide bond between cytochrome b and the iron-sulfur protein. *J. Biol. Chem. 275*, 38597−38604.
(12) Zhang, Z., Huang, L., Shulmeister, V. M., Chi, Y. I., Kim, K. K., Hung, L. W., Crofts, A. R., Berry, E. A., and Kim, S. H. (1998) Electron transfer by domain movement in cytochrome bc_1. *Nature 392*, 677−684.
(13) Brandt, U. (1998) The chemistry and mechanics of ubihydroquinone oxidation at center P (Qo) of the cytochrome bc1 complex. *Biochim. Biophys. Acta 1365*, 261−268.
(14) Engstrom, G., Xiao, K., Yu, C. A., Yu, L., Durham, B., and Millett, F. (2002) Photoinduced electron transfer between the Rieske iron-sulfur protein and cytochrome $c_{(1)}$ in the *Rhodobacter sphaeroides* cytochrome $bc_{(1)}$ complex. Effects of pH, temperature, and driving force. *J. Biol. Chem. 277*, 31072−31078.
(15) Iwata, S., Lee, J. W., Okada, K., Lee, J. K., Iwata, M., Rasmussen, B., Link, T. A., Ramaswamy, S., and Jap, B. K. (1998) Complete structure of the 11-subunit bovine mitochondrial cytochrome bc_1 complex. *Science 281*, 64−71.
(16) Darrouzet, E., Valkova-Valchanova, M., Moser, C. C., Dutton, P. L., and Daldal, F. (2000) Uncovering the [2Fe2S] domain movement in cytochrome bc1 and its implications for energy conversion. *Proc. Natl. Acad. Sci. U.S.A. 97*, 4567−4572.
(17) Conte, L., and Zara, V. (2011) The Rieske Iron-Sulfur Protein: Import and Assembly into the Cytochrome $bc_{(1)}$ Complex of Yeast Mitochondria. *Bioinorg. Chem. Appl. 2011*, 363941.
(18) Crofts, A. R., Lhee, S., Crofts, S. B., Cheng, J., and Rose, S. (2006) Proton pumping in the bc1 complex: A new gating mechanism that prevents short circuits. *Biochim. Biophys. Acta 1757*, 1019−1034.
(19) Berry, E. A., and Huang, L. S. (2011) Conformationally linked interaction in the cytochrome $bc_{(1)}$ complex between inhibitors of the $Q_{(o)}$ site and the Rieske iron-sulfur protein. *Biochim. Biophys. Acta 1807*, 1349−1363.
(20) Shen, Y., and Bax, A. (2010) Prediction of Xaa-Pro peptide bond conformation from sequence and chemical shifts. *J. Biomol. NMR 46*, 199−204.
(21) Schubert, M., Labudde, D., Oschkinat, H., and Schmieder, P. (2002) A software tool for the prediction of Xaa-Pro peptide bond conformations in proteins based on ^{13}C chemical shift statistics. *J. Biomol. NMR 24*, 149−154.
(22) Cheng, H., Westler, W. M., Xia, B., Oh, B. H., and Markley, J. L. (1995) Protein expression, selective isotopic labeling, and analysis of hyperfine-shifted NMR signals of *Anabaena* 7120 vegetative [2Fe-2S]ferredoxin. *Arch. Biochem. Biophys. 316*, 619−634.
(23) Markley, J. L., Bax, A., Arata, Y., Hilbers, C. W., Kaptein, R., Sykes, B. D., Wright, P. E., and Wüthrich, K. (1998) Recommendations for the presentation of NMR structures of proteins and nucleic acids. *J. Mol. Biol. 280*, 933−952.
(24) http://www.cgl.ucsf.edu/home/sparky.
(25) Machonkin, T. E., Westler, W. M., and Markley, J. L. (2002) $^{13}C\{^{13}C\}$ 2D NMR: A Novel Strategy for the Study of Paramagnetic Proteins with Slow Electronic Relaxation Rates. *J. Am. Chem. Soc. 124*, 3204−3205.
(26) Machonkin, T. E., Westler, W. M., and Markley, J. L. (2004) Strategy for the study of paramagnetic proteins with slow electronic relaxation rates by NMR spectroscopy: Application to oxidized human [2Fe-2S] ferredoxin. *J. Am. Chem. Soc. 126*, 5413−5426.
(27) Solmaz, S. R., and Hunte, C. (2008) Structure of complex III with bound cytochrome c in reduced state and definition of a minimal core interface for electron transfer. *J. Biol. Chem. 283*, 17542−17549.
(28) Esser, L., Quinn, B., Li, Y. F., Zhang, M., Elberry, M., Yu, L., Yu, C. A., and Xia, D. (2004) Crystallographic studies of quinol oxidation site inhibitors: A modified classification of inhibitors for the cytochrome $bc_{(1)}$ complex. *J. Mol. Biol. 341*, 281−302.
(29) Konkle, M. E., Muellner, S. K., Schwander, A. L., Dicus, M. M., Pokhrel, R., Britt, R. D., Taylor, A. B., and Hunsicker-Wang, L. M. (2009) Effects of pH on the Rieske protein from *Thermus thermophilus*: A spectroscopic and structural analysis. *Biochemistry 48*, 9848−9857.
(30) Hsueh, K. L., Westler, W. M., and Markley, J. L. (2010) NMR Investigations of the Rieske Protein from *Thermus thermophilus* Support a Coupled Proton and Electron Transfer Mechanism. *J. Am. Chem. Soc. 132*, 7908−7918.
(31) Zu, Y., Fee, J. A., and Hirst, J. (2001) Complete thermodynamic characterization of reduction and protonation of the $bc_{(1)}$-type Rieske [2Fe-2S] center of *Thermus thermophilus*. *J. Am. Chem. Soc. 123*, 9906−9907.
(32) Lin, I. J., Chen, Y., Fee, J. A., Song, J., Westler, W. M., and Markley, J. L. (2006) Rieske protein from *Thermus thermophilus*: ^{15}N NMR titration study demonstrates the role of iron-ligated histidines in the pH dependence of the reduction potential. *J. Am. Chem. Soc. 128*, 10672−10673.